SANDIA REPORT

SAND 2011-3865
Unlimited Release
Printed June, 2011

Control Volume Finite Element Method with Multidimensional Edge Element Scharfetter-Gummel upwinding. Part 1. Formulation

Pavel Bochev

Prepared by
Sandia National Laboratories
Albuquerque, New Mexico 87185 and Livermore, California 94550

Sandia National Laboratories is a multi-program laboratory managed and operated by Sandia Corporation, a wholly owned subsidiary of Lockheed Martin Corporation, for the U.S. Department of Energy's National Nuclear Security Administration under contract DE-AC04-94AL85000.

Issued by Sandia National Laboratories, operated for the United States Department of Energy by Sandia Corporation.

Available to DOE and DOE contractors from
U.S. Department of Energy
Office of Scientific and Technical Information
P.O. Box 62
Oak Ridge, TN 37831

Telephone: (865) 576-8401
Facsimile: (865) 576-5728
E-Mail: reports@adonis.osti.gov
Online ordering: http://www.osti.gov/bridge

Available to the public from
U.S. Department of Commerce
National Technical Information Service
5285 Port Royal Rd
Springfield, VA 22161

Telephone: (800) 553-6847
Facsimile: (703) 605-6900
E-Mail: orders@ntis.fedworld.gov
Online ordering: http://www.ntis.gov/help/ordermethods.asp?loc=7-4-0#online

SAND 2011-3865
Unlimited Release
Printed June, 2011

Control Volume Finite Element Method with Multidimensional Edge Element Scharfetter-Gummel upwinding. Part 1. Formulation

Pavel Bochev
Numerical Analysis and Applications, MS-1320
Sandia National Laboratories
Albuquerque, NM 87185-1320
pbboche@sandia.gov

Abstract

We develop a new formulation of the Control Volume Finite Element Method (CVFEM) with a multidimensional Scharfetter-Gummel (SG) upwinding for the drift-diffusion equations. The formulation uses standard nodal elements for the concentrations and expands the flux in terms of the lowest-order Nedelec $H(curl, \Omega)$-compatible finite element basis. The SG formula is applied to the edges of the elements to express the Nedelec element degree of freedom on this edge in terms of the nodal degrees of freedom associated with the endpoints of the edge. The resulting upwind flux incorporates the upwind effects from all edges and is defined at the interior of the element. This allows for accurate evaluation of integrals on the boundaries of the control volumes for arbitrary quadrilateral elements.

The new formulation admits efficient implementation through a standard loop over the elements in the mesh followed by loops over the element nodes (associated with control volume fractions in the element) and element edges (associated with flux degrees of freedom). The quantities required for the SG formula can be precomputed and stored for each edge in the mesh for additional efficiency gains. For clarity the details are presented for two-dimensional quadrilateral grids. Extension to other element shapes and three dimensions is straightforward.

Acknowledgment

The author acknowledges funding by the Advanced Simulation & Computing (ASC) program of the National Nuclear Security Administration (NNSA), and DOE's Office of Science Advanced Scientific Computing Research Program.

Contents

Nomenclature **7**

Introduction 9

Notation 10

The drift-diffusion model 10

The CVFEM for the drift-diffusion equations 11

The multi-dimensional CVFEM-SG formulation 13

The SG-BIM scheme 13

Extension of SG upwinding to the CVFEM 15

Multi-dimensional SG-upwind flux definition 16

Assembly of the CVFEM-SG stiffness matrix 18

References **19**

List of Figures

1 CVFEM is defined using an unstructured primal grid. The figure shows a typical CVFEM control volume C_i when the primal grid is comprised of quadrilaterals. For such grids the control volume C_i is a polygon. The number of sides in C_i depends on the number of primal edges having $\boldsymbol{v}_i$ as a vertex and can be as high as two times the number of these edges. Let ∂C_{ij} denote the union of the two dual sides (∂C_{ij}^s and ∂C_{ij}^t in the figure) which intersect edge $\boldsymbol{e}_{ij}$. For unstructured grids, the unit normals on these two sides are not guaranteed to be parallel to $\boldsymbol{e}_{ij}$. 12

2 BIM is defined using structured grids. The figure shows a typical BIM control volume C_i when the primal grid is comprised of rectangles. For such grids the control volume C_i is also a rectangle and the number of sides in C_i is always four. Every primal edge (side) $\boldsymbol{e}_{ij}$ is intersected by a single dual side ∂C_{ij} and $\partial C_{ij} \perp \boldsymbol{e}_{ij}$. BIM can be defined on Voronoy-Delaunay grids in which case the control volume C_i is a hexagon whose sides are perpendicular to the primal edges sharing vertex $\boldsymbol{v}_i$. 14

Nomenclature

Semiconductor equations

ψ - electric potential
n - electron concentration
p - hole concentration
C - doping profile
R - generation-recombination term.
λ - minimal Debye length of the device
D_n - electron diffusivity
D_p - hole diffusivity
μ_n - electron mobility
μ_p - hole mobility
$\mathbf{E}$ - electric field;
$\mathbf{J}_n$ - electron current density;
$\mathbf{J}_p$ - hole current density;

Discretization

Ω - computational domain in two dimensions.
$K_h(\Omega)$ - finite element mesh
K_s - finite element
$\boldsymbol{b}_s$ - barycenter of element K_s
$\boldsymbol{v}_i$ - a mesh vertex
$\boldsymbol{e}_{ij}$ - an edge with endpoints $\boldsymbol{v}_i$ and $\boldsymbol{v}_j$
$\boldsymbol{m}_{ij}$ - midpoint of edge $\boldsymbol{e}_{ij}$
$K(\boldsymbol{v}_i)$ - the set of all elements K_s having a common vertex $\boldsymbol{v}_i$.
$K(\boldsymbol{e}_{ij})$ - the set of all elements K_s having a common edge $\boldsymbol{e}_{ij}$.
$V(K_s)$ - the vertices of element K_s.
$E(K_s)$ - the edges (sides) of element K_s
C_i - control volume associated with vertex $\boldsymbol{v}_i$
∂C_{ij}^s - the side of C_i contained in element K_s which intersects edge $\boldsymbol{e}_{ij}$
$\boldsymbol{m}_{ij}^s$ - the midpoint of side ∂C_{ij}^s
∂C_{ij} - the union of the two sides of C_i which intersect edge $\boldsymbol{e}_{ij}$, i.e., $\partial C_{ij} = \partial C_{ij}^s \cup \partial C_{ij}^t$; $K_s, K_t \in K(\boldsymbol{e}_{ij})$
N_i - C^0 Lagrangian (nodal) basis function associated with vertex $\boldsymbol{v}_i$
$\vec{W}_{ij}$ - Lowest-order Nedelec edge element basis function associated with edge $\boldsymbol{e}_{ij}$

Introduction

Semiconductor devices are commonly modeled by Van Roosbroeck equations; see [6] or [5]. These equations are a coupled system of nonlinear PDE's, which describe the motion of charges in semiconductors. Accurate and stable numerical solution of the semiconductor equations requires discretization methods that

- conserve electron and hole current density;
- employ upwinding to handle the advective character of the equations

The Control Volume Finite Element Method (CVFEM) [2] fulfills the first condition. The CVFEM solution is expressed in terms of a finite element basis but the discrete equations are obtained by integrating the conservative form of the differential equations on control volumes surrounding the vertices of the finite element mesh. As a result, CVFEM is conservative with respect to the control volumes. The CVFEM approach combines features from finite volume methods (the use of a primal-dual grid complex) and finite elements (the use of piecewise polynomial basis functions for the approximate solution).

The Scharfetter-Gummel (SG) scheme [9] is a classical approach to solve the one-dimensional semiconductor equations, which satisfies the second requirement. The SG method is an exponentially fitted upwind difference scheme for the current continuity equations. Extensions of the SG scheme to unstructured grids usually follow two general paths. One path is to use exponentially fitted shape functions [1, 13, 14]. The exponential shape functions can be used within the CVFEM approach [12] in lieu of the standard nodal shape functions. However, exponential shape functions are generally not known explicitly and their evaluation requires solution of two-point boundary value problems on each element [13]. A second path is to extend SG by using methods such as SUPG [4] together with numerical diffusion defined by application of the SG scheme along local coordinate directions [11]. This approach is applicable to tensor product elements such as quadrilaterals and hexahedrons, but not to simplicial elements

In this report we develop a new CVFEM-SG formulation for the semiconductor equations with multidimensional upwinding based on the SG scheme. The key idea is to approximate the currents in the semiconductor equations using the lowest-order Nedelec $H(curl, \Omega)$-compatible finite element space (edge elements) [8]. The SG scheme is applied to the edges $\boldsymbol{e}_{ij}$ of element K_s to express the edge element degree of freedom for the current on $\boldsymbol{e}_{ij}$ in terms of the nodal degrees of freedom associated with the endpoints $\boldsymbol{v}_i$ and $\boldsymbol{v}_j$ of that edge. The resulting upwind flux incorporates the upwind effects from all edges in element K_s and is defined at any point in the interior of the element. This allows for accurate evaluation of integrals on the boundaries of the control volumes for arbitrary unstructured elements. In particular, accuracy is not lost when the part ∂C_{ij} of the control volume boundary, which intersects edge $\boldsymbol{e}_{ij}$ is comprised of two separate segments whose normals are not parallel to the edge; see Fig. 1.

The new CVFEM-SG formulation admits efficient implementation through a standard loop over the elements in the mesh followed by loops over the element nodes (associated with control volume fractions in the element) and element edges (associated with flux degrees of freedom). The only difference in the assembly process due to the use of edge elements for the flux is that the innermost loop generates contributions to two, as opposed to one, matrix entries. These contributions are scattered to entries with global column numbers corresponding to the global vertex numbers of

the edge's endpoints. Both entries have the same row number corresponding to the global vertex number of the vertex associated with the control volume.

The quantities required for the SG formula, such as the edge Reynolds number, can be precomputed in advance and stored for each edge in the mesh for additional efficiency gains. Because the new CVFEM-SG formulation uses Nedelec elements to represent the flux, it is applicable to any two or three-dimensional finite element partition.

Notation

Let Ω denote a bounded region in $\Re^n$ with boundary $\partial\Omega$. We assume that $\partial\Omega$ has two disjoint pieces denoted by Γ_D and Γ_N.

We use standard notations for Sobolev spaces $H^s(\Omega)$ of order s with inner product $(\cdot,\cdot)_s$ and norm $\|\cdot\|_s$, respectively. As usual, $L^2(\Omega)$ and $\mathbf{L}^2(\Omega)$ denote the spaces of all square integrable scalar and vector functions on Ω.

The drift-diffusion model

The nonlinear coupled drift-diffusion equations

$$\nabla\cdot(\lambda^2\mathbf{E}) - (p - n + C) = 0 \quad \text{and} \quad \mathbf{E} = -\nabla\psi \quad \text{in } \Omega \tag{1}$$

$$\frac{\partial n}{\partial t} - \nabla\cdot\mathbf{J}_n + R(\psi, n, p) = 0 \quad \text{and} \quad \mathbf{J}_n = \mu_n n\mathbf{E} + D_n\nabla n \quad \text{in } \Omega \tag{2}$$

$$\frac{\partial p}{\partial t} + \nabla\cdot\mathbf{J}_p + R(\psi, n, p) = 0 \quad \text{and} \quad \mathbf{J}_p = \mu_p p\mathbf{E} - D_p\nabla p \quad \text{in } \Omega \tag{3}$$

are a standard mathematical models for semiconductor devices [10]. The variables and material parameters in (1)–(3) are as follows

- ψ scalar electric potential;
- n: electron concentration;
- p: hole concentration;
- $\mathbf{E}$: electric field;
- $\mathbf{J}_n$: electron current density;
- $\mathbf{J}_p$: hole current density;
- λ: minimal Debye length of the device.
- D_n: electron diffusivity
- D_p: hole diffusivity
- μ_n: electron mobility
- μ_p: hole mobility

The system (1)–(3) is augmented with the boundary conditions

$$n = n_D \quad \text{and} \quad p = p_D \quad \text{on } \Gamma_D \tag{4}$$

$$\mathbf{J}_n \cdot \vec{\boldsymbol{n}} = 0 \quad \text{and} \quad \mathbf{J}_p \cdot \vec{\boldsymbol{n}} = 0 \quad \text{on } \Gamma_N. \tag{5}$$

Equation (1) is a simplified model of the electric field in the device and (2)–(3) are the continuity equations for the electron and hole currents. The terms $\mu_n n\mathbf{E}$ and $\mu_p p\mathbf{E}$ are advective fluxes, while $D_n\nabla n$ and $D_p\nabla p$ are diffusive fluxes. When the electron and hole drift velocities

$$\mathbf{u}_n = \mu_n\mathbf{E} \quad \text{and} \quad \mathbf{u}_p = \mu_p\mathbf{E} \tag{6}$$

dominate the diffusive fluxes, the continuity equations have a pronounced advection-dominated character.

The CVFEM for the drift-diffusion equations

The CVFEM is a hybrid method which combines representation of the discrete solution in terms of a finite element basis with definition of the discrete equations through integration of conservative form of the governing equations on dual volumes C_i associated with the vertices $\boldsymbol{v}_i$ of the finite element mesh $K_h(\Omega)$.

For clarity we present details when Ω is two-dimensional and $K_h(\Omega)$ is a conforming finite element partition of Ω into quadrilateral elements. Extension to other element shapes and three dimensions is straightforward. For quadrilateral grids the control volume C_i corresponding to vertex $\boldsymbol{v}_i$ is constructed as follows. For every element K_r which has $\boldsymbol{v}_i$ as a vertex, i.e., for every $K_r \in K(\boldsymbol{v}_i)$, we connect its barycenter $\boldsymbol{b}_r$ with the midpoints $\boldsymbol{m}_{ik}$ and $\boldsymbol{m}_{il}$ of the two edges coming out of $\boldsymbol{v}_i$; see Fig. 1. This construction guarantees that $\boldsymbol{v}_i \in C_i$ whenever the grid is comprised of convex but not necessarily uniform quadrilaterals. We will require some additional notation for the CVFEM method.

- $\partial\dot{C}_i = \partial C_i \cap \dot{\Omega}$ is the intersection of the control volume boundary with the interior of Ω
- $\partial C_i^N = \partial C_i \cap \Gamma_N$ is the control volume boundary located on the Neumann portion of $\partial\Omega$

The new CVFEM-SG formulation combines the CVFEM with a novel extension of the one-dimensional SG upwind scheme to unstructured grids. To explain the key ideas it suffices to consider a single continuity equation. We choose to work with the electron continuity equation

$$\begin{cases} \dfrac{\partial n}{\partial t} - \nabla\cdot\mathbf{J}_n + R(\psi,n,p) = 0 \quad \text{and} \quad \mathbf{J}_n = \mu_n n\mathbf{E} + D_n\nabla n \\ \qquad\qquad n = g \quad \text{on } \Gamma_D \quad \text{and} \quad \mathbf{J}_n\cdot\vec{\boldsymbol{n}} = h \quad \text{on } \Gamma_N \end{cases} \tag{7}$$

with the assumption that ψ and p are given functions and $\mathbf{E} = -\nabla\psi$. For simplicity we will omit the subscript n when there's no danger of confusion.

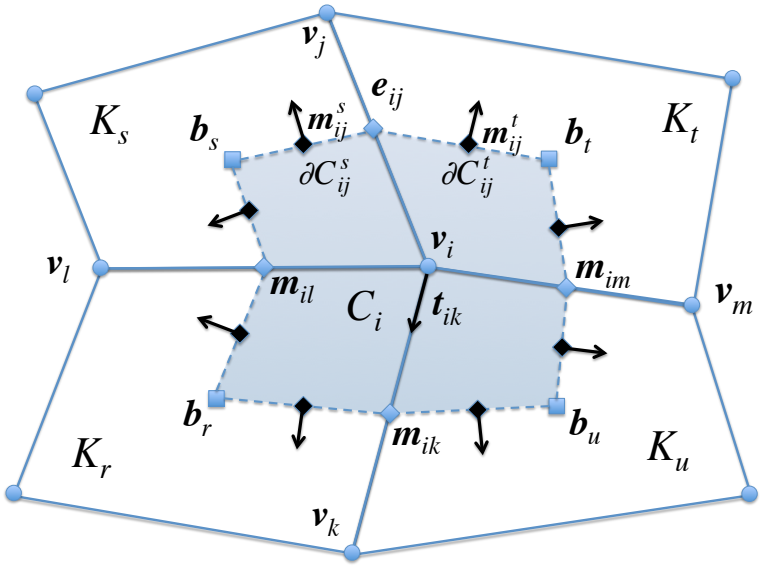

Figure 1: CVFEM is defined using an unstructured primal grid. The figure shows a typical CVFEM control volume C_i when the primal grid is comprised of quadrilaterals. For such grids the control volume C_i is a polygon. The number of sides in C_i depends on the number of primal edges having $\boldsymbol{v}_i$ as a vertex and can be as high as two times the number of these edges. Let ∂C_{ij} denote the union of the two dual sides (∂C_{ij}^s and ∂C_{ij}^t in the figure) which intersect edge $\boldsymbol{e}_{ij}$. For unstructured grids, the unit normals on these two sides are not guaranteed to be parallel to $\boldsymbol{e}_{ij}$.

In the CVFEM approach we integrate the governing equation (7) over each control volume C_i and apply the Divergence theorem to obtain the "weak" form

$$\int_{C_i} \frac{\partial n}{\partial t}\, dV - \int_{\partial \dot{C}_i} (\mu_n n \mathbf{E} + D_n \nabla n) \cdot \vec{\boldsymbol{n}}\, dS = \int_{C_i} R(\psi, n, p) dV + \int_{\partial C_i^N} h\, dS\,. \tag{8}$$

To derive the corresponding discrete equation we approximate n by the C^0 nodal bilinear space Q_1. Let $\{N_i\}$ be the standard Lagrangian basis for Q_1 constructed on the mesh $K_h(\Omega)$. With some abuse of notation we write $i \in \dot{\Omega} \cup \Gamma_N$ when vertex $\boldsymbol{v}_i$ is in the interior of Ω or on the Neumann portion of the boundary. Likewise, we write $i \in \Gamma_D$ if the vertex is on the Dirichlet part of the boundary. Using these conventions the finite element solution can be expressed as two separate sums over nodes associated with the unknowns and nodes on the Dirichlet boundary:

$$n_h(\boldsymbol{x}, t) = \sum_{j \in \dot{\Omega} \cup \Gamma_N} n_j(t) N_j(\boldsymbol{x}) + \sum_{j \in \Gamma_D} g(\boldsymbol{v}_j, t) N_j(\boldsymbol{x})\,. \tag{9}$$

After substituting (9) in (8) we obtain the semi-discrete in space problem

$$\begin{aligned} &\sum_{j \in \dot{\Omega} \cup \Gamma_N} \frac{\partial n_j(t)}{\partial t} \int_{C_i} N_j\, dV - \sum_{j \in \dot{\Omega} \cup \Gamma_N} n_j(t) \int_{\partial \dot{C}_i} (\mu_n N_j \mathbf{E} + D_n \nabla N_j) \cdot \vec{\boldsymbol{n}}\, dS \\ &\quad = \int_{C_i} R(\psi, n_h, p) dV + \int_{\partial C_i^N} h\, dS + \sum_{j \in \Gamma_D} g(\boldsymbol{v}_j, t) \int_{\partial \dot{C}_i} (\mu_n N_j \mathbf{E} + D_n \nabla N_j) \cdot \vec{\boldsymbol{n}}\, dS \end{aligned} \tag{10}$$

Discretization of the time derivative yields the fully discrete problem.

Remark 1. *Similar to conventional finite elements, the CVFEM formulation (10) gives rise to a linear system of algebraic equations for the unknown coefficients* $\{n_j\}_{j\in\dot{\Omega}\cup\Gamma_N}$. *Each row in the CVFEM linear system corresponds to a control volume* C_i, *which surrounds a vertex* $\boldsymbol{v}_i$ *associated with an unknown nodal value* n_i. *As a result, the CVFEM linear system has the same sparsity pattern as the standard finite element system. For example, the second term in (10) defines a CVFEM analogue of the finite element stiffness matrix with element* ij *given by*

$$K_{ij} = \int_{\partial\dot{C}_i} (\mu_n N_j \mathbf{E} + D_n \nabla N_j) \cdot \vec{\boldsymbol{n}}\, dS\,; \quad i,j \in \dot{\Omega}\cup\Gamma_N \tag{11}$$

The vectors of unknown and Dirichlet nodal coefficients are $\vec{n}$ and $\vec{g}$, respectively:

$$\vec{n} = \{n_i\}; i \in \dot{\Omega}\cup\Gamma_N \quad \text{and} \quad \vec{g} = \{g(\boldsymbol{v}_i,t); i\in\Gamma_D\,.$$

The CVFEM formulation (10) employs the nodal numerical flux

$$\mathbf{J}_h = \mu_n \mathbf{E} N_j + D_n \nabla N_j \tag{12}$$

which acts on a single nodal value n_j. This flux is not appropriate when electron drift velocity $\mu_n\mathbf{E}$ is much larger than electron diffusivity D_n. It is well-known that advection-dominated problems require some form of upwinding for numerical stability. To this end we will replace the nodal numerical flux $\mathbf{J}_h$ in (10) with an upwind numerical flux $\widehat{\mathbf{J}}_h(\vec{n},\vec{g})$, which acts on multiple nodal values of the electron concentration:

$$\sum_{j\in\dot{\Omega}\cup\Gamma_N} \frac{\partial n_j(t)}{\partial t} \int_{C_i} N_j\, dV - \int_{\partial\dot{C}_i} \widehat{\mathbf{J}}_h(\vec{n},\vec{g})\cdot\vec{\boldsymbol{n}}\, dS = \int_{C_i} R(\psi,n_h,p) dV + \int_{\partial C_i^N} h\, dS\,. \tag{13}$$

Below we develop a new CVFEM-SG formulation which extends the classical SG scheme to arbitrary unstructured elements. The key idea is to use $H(curl,\Omega)$-conforming edge elements for $\widehat{\mathbf{J}}_h$ to obtain a multi-dimensional extension of the SG scheme. SG is applied to the edges of each element to express edge degrees of freedom in terms of upwind nodal degrees of freedom.

The multi-dimensional CVFEM-SG formulation

In this section we formulate a multi-dimensional generalization of the SG scheme and use it to define the new CVFEM-SG method. To motivate the approach we first examine the extension of the one-dimensional Scharfetter–Gummel upwind scheme to the Box Integration Method (BIM) on rectangular grids [3, 10]. This extension provides a useful template for the CVFEM because both methods use primal-dual grids and define the discrete equations by integration over the control (dual) volumes. As a result, both BIM and CVFEM require upwind fluxes on the boundary ∂C_i of each control volume C_i.

The SG-BIM scheme

In the BIM the integral over ∂C_i is approximated by the midpoint rule applied to each side of the control volume. Specifically, let ∂C_{ij} be the side of C_i which intersects edge $\boldsymbol{e}_{ij}$ at its midpoint $\boldsymbol{m}_{ij}$;

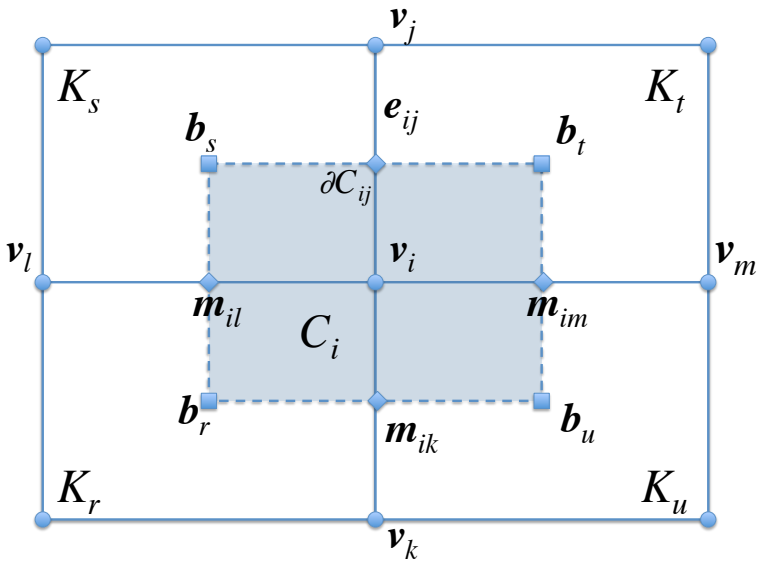

Figure 2: BIM is defined using structured grids. The figure shows a typical BIM control volume C_i when the primal grid is comprised of rectangles. For such grids the control volume C_i is also a rectangle and the number of sides in C_i is always four. Every primal edge (side) $\boldsymbol{e}_{ij}$ is intersected by a single dual side ∂C_{ij} and $\partial C_{ij} \perp \boldsymbol{e}_{ij}$. BIM can be defined on Voronoy-Delaunay grids in which case the control volume C_i is a hexagon whose sides are perpendicular to the primal edges sharing vertex $\boldsymbol{v}_i$.

see Fig. 2. Application of the midpoint rule for the integral on this side yields the approximation

$$\int_{\partial C_{ij}} \mathbf{J} \cdot \vec{\boldsymbol{n}}\, dS \approx |\partial C_{ij}|\, \langle \mathbf{J} \cdot \vec{\boldsymbol{n}} \rangle_{ij} \ . \tag{14}$$

where $\langle \mathbf{J} \cdot \vec{\boldsymbol{n}} \rangle_{ij}$ is the normal component of $\mathbf{J}$ to ∂C_{ij}, evaluated at the midpoint $\boldsymbol{m}_{ij}$. Because the normal to side ∂C_{ij} of the control volume is parallel to edge $\boldsymbol{e}_{ij}$, BIM approximates the value of $\langle \mathbf{J} \cdot \vec{\boldsymbol{n}} \rangle_{ij}$ by the value of the outgoing current density J_{ij} along edge $\boldsymbol{e}_{ij}$ at $\boldsymbol{m}_{ij}$. To estimate J_{ij} at the midpoint $\boldsymbol{m}_{ij}$ BIM uses a procedure proposed by Scharfetter and Gummel [9]. The SG approach estimates the edge current J_{ij} along $\boldsymbol{e}_{ij}$ by solving a simplified version of the current continuity equation (7) restricted to edge $\boldsymbol{e}_{ij}$:

$$\frac{dn}{dt} - \frac{dJ_{ij}}{ds} + R = 0; \quad J_{ij} = \mu_n \mathbf{E}_{ij} n + D_n \frac{dn}{ds}; \quad \mathbf{E}_{ij} = -\frac{d\psi}{ds}\,. \tag{15}$$

Problem (15) is an ordinary differential equation (ODE). The variable s is the edge parametrization by length. The simplifications used by Scharfetter and Gummel allow to solve this ODE in closed form and express J_{ij} in terms of the nodal values at the endpoints of $\boldsymbol{e}_{ij}$. The simplification steps are as follows.

Step 1 Assume that n is time-independent and neglect the recombination term. This simplifies equation (15) to

$$\frac{dJ_{ij}}{ds} = 0; \quad J_{ij} = \mu_n \mathbf{E}_{ij} n + D_n \frac{dn}{ds}\,,$$

and implies that $J_{ij} = const$ along the edge.

Step 2 Assume that μ_n and D_n are connected through the Einstein relation

$$\mu_n = \frac{D_n}{\beta} \quad \text{where} \quad \beta = \frac{kT_0}{q}\,. \tag{16}$$

This further simplifies the ODE for the edge current to

$$J_{ij} = D_n \left(\frac{\mathbf{E}_{ij}}{\beta} n + \frac{dn}{ds} \right) . \tag{17}$$

Step 3 Assume that the electric potential ψ varies linearly along $\boldsymbol{e}_{ij}$ so that

$$\mathbf{E}_{ij} = -\frac{(\psi_j - \psi_i)}{|\boldsymbol{e}_{ij}|}\,; \quad \psi_i = \psi(\boldsymbol{v}_i);\ \psi_j = \psi(\boldsymbol{v}_j)\,,$$

and solve (17) to express J_{ij} in terms of the values n_i, n_j of n at the endpoints of $\boldsymbol{e}_{ij}$. The result is the SG formula:

$$J_{ij} = \frac{D_n}{|\boldsymbol{e}_{ij}|} \Big[n_j B(-2a_{ij}) - n_i B(2a_{ij}) \Big] \tag{18}$$

where

$$a_{ij} = -\frac{(\psi_j - \psi_i)}{2\beta}$$

is the edge Reynolds number, and

$$B(x) = \frac{x}{\exp(x) - 1}$$

is the Bernoulli function.

In summary, in the BIM using the SG procedure to estimate the normal flux at the midpoints of the control volume sides yields the following formula for the integral on ∂C_{ij}:

$$\int_{\partial C_{ij}} \mathbf{J} \cdot \vec{\boldsymbol{n}}\, dS \approx \frac{D_n}{|\boldsymbol{e}_{ij}|} \Big[n_j B(-2a_{ij}) - n_i B(2a_{ij}) \Big] |\partial C_{ij}|\,. \tag{19}$$

Extension of SG upwinding to the CVFEM

The key difference that complicates the extension of the SG approach to the CVFEM case is that BIM uses *topologically dual grids*[1] for which the sides of C_i are perpendicular to the primal edges, whereas in the CVFEM the grids are not topologically dual and the sides of C_i are not necessarily perpendicular to the primal edges.

To explain the difficulties caused by the lack of topological duality in the CVFEM let ∂C_{ij}^s and ∂C_{ij}^t denote the two sides of C_i associated with the primal edge $\boldsymbol{e}_{ij}$; see Fig. 1 and set $\partial C_{ij} = \partial C_{ij}^s \cup \partial C_{ij}^t$. As a result, the CVFEM analogue of (14) is

[1]We remind that two grids in d-dimensions are topologically dual if there is one-to-one correspondence between their k and $d-k$-dimensional entities. For example, in three dimensions ($d = 3$) every primal vertex ($k = 0$) corresponds to a unique dual cell ($3-0=3$); every primal edge ($k = 1$) corresponds to a unique dual face ($3-1=2$), every primal face ($k = 2$) corresponds to a unique dual edge ($3-2=1$), and every primal cell ($k = 3$) corresponds to a unique dual vertex ($3-3=0$). In two dimensions ($d = 2$) the correspondence is between primal vertices ($k = 0$) and dual cells ($2-0=2$), primal sides ($k = 1$) and dual sides ($2-1=2$) and primal cells ($k = 2$) and dual vertices ($2-2=0$).

$$\int_{\partial C_{ij}} \mathbf{J}\cdot\vec{\boldsymbol{n}}\,dS = \int_{\partial C^s_{ij}} \mathbf{J}\cdot\vec{\boldsymbol{n}}\,dS + \int_{\partial C^t_{ij}} \mathbf{J}\cdot\vec{\boldsymbol{n}}\,dS \approx |\partial C^s_{ij}|\,\langle \mathbf{J}\cdot\vec{\boldsymbol{n}}\rangle^s_{ij} + |\partial C^t_{ij}|\,\langle \mathbf{J}\cdot\vec{\boldsymbol{n}}\rangle^t_{ij}\ , \tag{20}$$

where $\langle \mathbf{J}\cdot\vec{\boldsymbol{n}}\rangle^s_{ij}$ and $\langle \mathbf{J}\cdot\vec{\boldsymbol{n}}\rangle^t_{ij}$ are the normal components of $\mathbf{J}$ on ∂C^s_{ij} and ∂C^t_{ij}, evaluated at the midpoints $\boldsymbol{m}^s_{ij}$ and $\boldsymbol{m}^t_{ij}$ of these sides, respectively.

If the unit normals on ∂C^s_{ij} and ∂C^t_{ij} are nearly parallel to $\boldsymbol{e}_{ij}$, they can be approximated by the unit tangent $\vec{\boldsymbol{t}}_{ij}$ to this edge. As a result,

$$|\partial C^s_{ij}|\,\langle \mathbf{J}\cdot\vec{\boldsymbol{n}}\rangle^s_{ij} + |\partial C^t_{ij}|\,\langle \mathbf{J}\cdot\vec{\boldsymbol{n}}\rangle^t_{ij} \approx (|\partial C^s_{ij}| + |\partial C^t_{ij}|)\langle \mathbf{J}\cdot\vec{\boldsymbol{t}}_{ij}\rangle_{ij} \tag{21}$$

where, similar to the BIM case, $\langle \mathbf{J}\cdot\vec{\boldsymbol{t}}_{ij}\rangle_{ij}$ is evaluated at the midpoint $\boldsymbol{m}_{ij}$ of edge $\boldsymbol{e}_{ij}$. In this case the integrals on the sides of the control volumes in the CVFEM can be approximated using the same edge values as in the BIM:

$$\int_{\partial C_{ij}} \mathbf{J}\cdot\vec{\boldsymbol{n}}\,dS \approx \frac{D_n}{|\boldsymbol{e}_{ij}|}\Big[n_j B(-2a_{ij}) - n_i B(2a_{ij})\Big]\,\big(|\partial C^s_{ij}| + |\partial C^s_{ij}|\big)\ . \tag{22}$$

Multi-dimensional SG-upwind flux definition

When the normals on ∂C^s_{ij} and ∂C^t_{ij} deviate significantly from the unit tangent $\vec{\boldsymbol{t}}_{ij}$ on $\boldsymbol{e}_{ij}$, then the right hand sides in (21) and (22) yield poor approximation of the integral on $\partial C_{ij} = \partial C^s_{ij} \cup \partial C^t_{ij}$. The key reason is that for such control volumes the tangential component of the current $\langle \mathbf{J}\cdot\vec{\boldsymbol{t}}_{ij}\rangle_{ij}$ along $\boldsymbol{e}_{ij}$ is poor approximation of the normal components $\langle \mathbf{J}\cdot\vec{\boldsymbol{n}}\rangle^s_{ij}$ and $\langle \mathbf{J}\cdot\vec{\boldsymbol{n}}\rangle^t_{ij}$ on the sides of the control volume.

A CVFEM formulation, which remains robust and accurate for a wide range of control volume shapes, requires accurate estimates of the normal flux components $\langle \mathbf{J}\cdot\vec{\boldsymbol{n}}\rangle^s_{ij}$ on the sides ∂C^s_{ij} of the control volumes. In the absence of topological duality it is clear that this cannot be accomplished by using the SG current density estimates on $\boldsymbol{e}_{ij}$ alone, and that the estimates from all edges in element K_s must be incorporated in the approximation of $\langle \mathbf{J}\cdot\vec{\boldsymbol{n}}\rangle^s_{ij}$.

To this end, we propose to expand the current density on K_s in terms of the lowest-order Nedelec edge element space [7, 8]

$$\widehat{\mathbf{J}}_h = \sum_{\boldsymbol{e}_{ij}\in E(K_s)} \alpha_{ij}\vec{W}_{ij}(\boldsymbol{x})\,. \tag{23}$$

The multi-dimensional extension of the SG scheme results from its application to the edges of K_s in order to express the flux coefficients α_{ij} in terms of the unknown nodal values n_i, n_{ij} of the electron concentration at the edge endpoints. We assume that the Nedelec basis function $\vec{W}_{ij}$ for edge $\boldsymbol{e}_{ij}$ is normalized to have a unit tangent component at the midpoint of $\boldsymbol{e}_{ij}$ and zero tangent component on all other edges:

$$\vec{W}_{ij}\cdot\vec{\boldsymbol{t}}_{kl} = \delta^{kl}_{ij};\quad \vec{\boldsymbol{t}}_{kl} = \boldsymbol{e}_{kl}/|\boldsymbol{e}_{kl}|$$

Using the basis normalization with (23) and accounting for the fact that $\mathbf{J} = \mu_n\mathbf{E}n + D_n\nabla n$ gives

$$\alpha_{ij} = \widehat{\mathbf{J}}_h\cdot\vec{\boldsymbol{t}}_{ij} \approx (\mu_n\mathbf{E}n + D_n\nabla n)\cdot\vec{\boldsymbol{t}}_{ij} = \mu_n\mathbf{E}_{ij}n(s) + D_n\frac{dn}{ds}\,.$$

In other words, the degrees of freedom in (23) approximate the outgoing current densities along the edges of K_s. The key idea is to use the SG scheme (18) to estimate edge currents on the edges of K_s, i.e., set the edge degrees of freedom in (23) according to (18):

$$\alpha_{ij} = \frac{D_n}{|\boldsymbol{e}_{ij}|}\Big[n_j B(-2a_{ij}) - n_i B(2a_{ij})\Big]\,.$$

As a result, the flux representation (23) for element K_s specializes to

$$\widehat{\mathbf{J}}_h = \sum_{\boldsymbol{e}_{ij}\in E(K_s)} \frac{D_n}{|\boldsymbol{e}_{ij}|}\Big[n_j B(-2a_{ij}) - n_i B(2a_{ij})\Big]\vec{W}_{ij}(\boldsymbol{x})\,. \tag{24}$$

Formula (24) gives the multi-dimensional extension of the SG scheme. It defines a vector field that can be evaluated at any point in element K_s. In the interior of K_s this field incorporates the upwinding effect from all edges in K_s because the Nedelec basis functions do not vanish at the interior points.

To obtain the new CVFEM-SG formulation we use the upwind flux defined by (24) in the CVFEM "weak" equation (13):

$$\begin{aligned}\sum_{j\in\dot{\Omega}\cup\Gamma_N} \frac{\partial n_j(t)}{\partial t}\int_{C_i} N_j\,dV - \sum_{\boldsymbol{e}_{kl}\in E(\Omega)}\left[\frac{D_n}{|\boldsymbol{e}_{kl}|}\Big[n_l B(-2a_{kl}) - n_k B(2a_{kl})\Big]\int_{\partial\dot{C}_i}\vec{W}_{kl}\cdot\vec{\boldsymbol{n}}\,dS\right]\\ = \int_{C_i} R(\psi,n_h,p)dV + \int_{\partial C_i^N} h\,dS\,,\end{aligned} \tag{25}$$

The second term in (25) incorporates the multi-dimensional SG upwinding. Note that while the sum in this term is over the edges, it operates on the nodal degrees of freedom. As a result, the CVFEM-SG "stiffness" matrix $\widehat{K}$ corresponding to the second term acts on the vector $\vec{n}$ of the unknown nodal values of the electron concentration. This fact can be further elucidated by rewriting the second term as double sum:

$$\begin{aligned}\sum_{j\in\dot{\Omega}\cup\Gamma_N} \frac{\partial n_j(t)}{\partial t}\int_{C_i} N_j\,dV + \sum_{j\in\dot{\Omega}\cup\Gamma_N} n_j\left[\sum_{\boldsymbol{e}_{kj}\in E(\boldsymbol{v}_j)}\left[\frac{\sigma_{kj}D_n}{|\boldsymbol{e}_{kj}|}B(2\sigma_{kj}a_{kj})\int_{\partial\dot{C}_i}\vec{W}_{kj}\cdot\vec{\boldsymbol{n}}\,dS\right]\right]\\ = \int_{C_i} R(\psi,n_h,p)dV + \int_{\partial C_i^N} h\,dS\,,\end{aligned} \tag{26}$$

where $\sigma_{kj} = \pm 1$ depends on the edge orientation:

$$\sigma_{kj} = \begin{cases} -1 & \text{if } \boldsymbol{e}_{kj} \text{ is oriented } \boldsymbol{v}_k \to \boldsymbol{v}_j \\ +1 & \text{if } \boldsymbol{e}_{kj} \text{ is oriented } \boldsymbol{v}_k \leftarrow \boldsymbol{v}_j \end{cases}$$

Formulae (25) and (26) are completely equivalent but differ in the type of inner-most loops required for assembly of the stiffness matrix $\widehat{K}$ and in the number of matrix entries they contribute to. If assembly is performed using (25), then the inner-most loop is over the local element edges, and the second term in (25) contributes simultaneously to

$$\widehat{K}_{ik} = \frac{D_n}{|\boldsymbol{e}_{kl}|}B(2a_{kl})\int_{\partial\dot{C}_i}\vec{W}_{kl}\cdot\vec{\boldsymbol{n}}\,dS \quad\text{and}\quad \widehat{K}_{il} = -\frac{D_n}{|\boldsymbol{e}_{kl}|}B(-2a_{kl})\int_{\partial\dot{C}_i}\vec{W}_{kl}\cdot\vec{\boldsymbol{n}}\,dS\,. \tag{27}$$

If, on the other hand one assembles $\widehat{K}_{ik}$ using (26), the inner-most loop is over the local element vertices and the second term in (26) contributes only to

$$\widehat{K}_{ij} = \sum_{\boldsymbol{e}_{kj} \in E(\boldsymbol{v}_j)} \left[\frac{\sigma_{kj} D_n}{|\boldsymbol{e}_{kj}|} B(2\sigma_{kj} a_{kj}) \int_{\partial \dot{C}_i} \vec{W}_{kj} \cdot \vec{\boldsymbol{n}} \, dS \right] \tag{28}$$

The matrix $\widehat{K}$ is an "upwind" version of the "stiffness" matrix (11), corresponding to the nodal flux (12). This follows from the fact that bilinear nodal elements and the lowest order edge elements on quadrilaterals belong to an exact sequence. As a result, gradients of nodal shape functions are linear combinations of the edge element basis functions:

$$\nabla N_j = \sum_{\boldsymbol{e}_{kl}} \mu_{kl} \vec{W}_{kl}$$

where $\mu_{kl} = \pm 1$ depends on edge orientations.

Assembly of the CVFEM-SG stiffness matrix

For efficient assembly of the CVFEM stiffness matrix $\widehat{K}$ the edge Reynolds numbers a_{kl} can be precomputed and stored in advance. Assembly of $\widehat{K}$ can then proceed according to the edge-based formula (27) or the node-based formula (28). The first formula requires three nested loops over the elements, the local element vertices and the local element edges. In the second formula the inner-most loop is over the local vertices and is not much different (except for the actual formula used) from the assembly of the "standard" CVFEM stiffness matrix (11)

For this reason we only review the assembly process using (27) because it requires inner loops over different mesh entities. This is typical for mixed methods but is somewhat unusual for formulations involving a single discrete field, such as the CVFEM or the Galerkin finite element method.

To assemble $\widehat{K}$ using (28) we first loop over all elements in the mesh. Given an element K_s we then loop over its local vertices $\boldsymbol{v}_i$, $i = 1, \ldots, N_{lv}$. This loop selects the control volume fraction $C_i \cap K_s$ of C_i, which is contained in the current element. The global index of the associated vertex $\boldsymbol{v}_i$ gives the global row number in $\widehat{K}$.

The inner-most loop is over the local edges $\boldsymbol{e}_{kl}$ of K_s. In this loop we compute the contribution to the integral over ∂C_i from element K_s

$$\widehat{K}_{ik} \mathrel{+}= \frac{D_n}{|\boldsymbol{e}_{kl}|} B(2a_{kl}) \int_{\partial \dot{C}_i \cap K_s} \vec{W}_{kl} \cdot \vec{\boldsymbol{n}} \, dS \quad \text{and} \quad \widehat{K}_{il} \mathrel{+}= -\frac{D_n}{|\boldsymbol{e}_{kl}|} B(-2a_{kl}) \int_{\partial \dot{C}_i \cap K_s} \vec{W}_{kl} \cdot \vec{\boldsymbol{n}} \, dS \,. \tag{29}$$

The global numbers of the endpoints $\boldsymbol{v}_k$ and $\boldsymbol{v}_l$ of edge $\boldsymbol{e}_{kl}$ give the global column numbers in the discretization matrix. If one or both of the endpoints of $\boldsymbol{e}_{kl}$ are on the Dirichlet boundary Γ_D, the contribution from this vertex times the boundary value is subtracted from the right hand side:

$$\boldsymbol{f}_i \mathrel{-}= g(\boldsymbol{v}_k) \frac{D_n}{|\boldsymbol{e}_{kl}|} B(2a_{kl}) \int_{\partial \dot{C}_i} \vec{W}_{kl} \cdot \vec{\boldsymbol{n}} \, dS \quad \text{and/or} \quad \boldsymbol{f}_i \mathrel{-}= -g(\boldsymbol{v}_l) \frac{D_n}{|\boldsymbol{e}_{kl}|} B(-2a_{kl}) \int_{\partial \dot{C}_i} \vec{W}_{kl} \cdot \vec{\boldsymbol{n}} \, dS \,.$$

References

[1] Lutz Angermann and Song Wang. Three-dimensional exponentially fitted conforming tetrahedral finite elements for the semiconductor continuity equations. *Applied Numerical Mathematics*, 46(1):19 – 43, 2003.

[2] B.R. Baliga and S.V Patankar. New finite element formulation for convection-diffusion problems. *Numerical Heat Transfer*, 3(4):393–409, October 1980.

[3] G. Ghione and A. Benvenuti. Discretization schemes for high-frequency semiconductor device models. *Antennas and Propagation, IEEE Transactions on*, 45(3):443 –456, March 1997.

[4] T. J. R. Hughes and A. Brooks. A theoretical framework for Petrov-Galerkin methods with discontinuous weighting functions: Application to the streamline-upwind procedure. In R. H. Gallagher et al, editor, *Finite Elements in Fluids*, volume 4, pages 47–65, New York, 1982. J. Wiley & Sons.

[5] P. Markowich. *The stationary semiconductor device equations*. Springer Verlag, Berlin, 1986.

[6] M. Mock. *Analysis of mathematical models of semiconductor devices*. Boole Press, Dublin, 1983.

[7] J. C. Nédélec. Mixed finite elements in $\mathbf{R}^3$. *Numerische Mathematik*, 35:315–341, 1980.

[8] J. C. Nédélec. A new family of finite element methods in $\mathbf{R}^3$. *Numerische Mathematik*, 50:57–81, 1986.

[9] D.L. Scharfetter and H.K. Gummel. Large-signal analysis of a silicon read diode oscillator. *Electron Devices, IEEE Transactions on*, 16(1):64 – 77, jan 1969.

[10] S. Selberherr. *Analysis and simulation of semiconductor devices*. Springer-Verlag, Berlin, 1984.

[11] M. Sharma and G.F. Carey. Semiconductor device simulation using adaptive refinement and flux upwinding. *Computer-Aided Design of Integrated Circuits and Systems, IEEE Transactions on*, 8(6):590 –598, June 1989.

[12] C. R. Swaminathan, V. R. Voller, and S. V. Patankar. A streamline upwind control volume finite element method for modeling fluid flow and heat transfer problems. *Finite Elements in Analysis and Design*, 13(2-3):169 – 184, 1993.

[13] Song Wang. A novel exponentially fitted triangular finite element method for an advection-diffusion problem with boundary layers. *Journal of Computational Physics*, 134(2):253 – 260, 1997.

[14] Song Wang. A new exponentially fitted triangular finite element method for the continuity equations in the drift-diffusion model of semiconductor devices. *M2AN*, 33(1):99–112, 1999.

DISTRIBUTION:

1 Max Gunzburger
Francis Eppes Distinguished Professor of Mathematics
School of Computational Science
400 Dirac Science Library
Florida State University Tallahassee, FL 32306-4120

1 Donald Estep
Department of Mathematics
Colorado State University
Fort Collins, Colorado 80523

1 Another Address
On a street
City, State
U.S.A.

1	MS 1320	John Aidun, 1445
2	MS 1320	Pavel Bochev, 1442
1	MS 1320	Scott Collis, 1442
1	MS 1320	Eric Cyr, 1426
1	MS 1541	Stefan Domino, 1541
1	MS 0316	Garry Hennigan, 1425
1	MS 1318	Rob Hoekstra, 1426
1	MS 0316	Larry Musson, 1425
1	MS 1320	John Shadid, 1444
1	MS 0316	Tom Smith, 1442
1	MS 1320	Roger Pawlowski, 1444
2	MS 1320	Denis Ridzal, 1441
1	MS 1318	Bart van Bloemen Waanders, 1442
1	MS 9409	Greg Wagner, 8365
1	MS 0380	David Womble, 1540
2	MS 0612	Review & Approval Desk, 4916
1	MS 0899	Technical Library, 9536 (electronic)


Sandia National Laboratories